

Depth-consistent P- and S-wave velocity reflection tomography using PP and PS seismic data

Stig-Kyrre Foss*, Statoil Research, Norway, and Bjørn Ursin, Department of Petroleum Engineering and Applied Geophysics, NTNU, Norway, and Maarten V. de Hoop, Center for Wave Phenomena, Colorado School of Mines, USA

Abstract

By a combination of the differential semblance misfit function to obtain uniform common image-point gathers and a co-depting procedure by map migration we obtain smooth velocity models yielding depth-consistent PP and PS images. A strategy is presented using these tools to obtain estimates of all parameters in a transversely isotropic media with a known symmetry axis. The strategy is illustrated on a North Sea OBS data set.

Introduction

The velocity-depth ambiguity in depth migration is a well known problem stemming from several factors such as, limited aperture, band-limitation of the source and the interplay between parameters of the background medium contributing to the non-uniqueness of the problem. In addition, the isotropic assumption can cause severe depth errors in the presence of anisotropy. These issues should be considered for PP and PS images from depth migration where geologically equivalent horizons should be imaged at the same depths. The present method is based upon the differential semblance misfit function in angle to find fitting background models (Symes and Carazzone, 1991). This requires amplitude-compensated angle-domain common image-point gathers (cigs) (Brandsberg-Dahl et al., 2003) to be uniform, i.e. constant amplitude for all angles and azimuths. Depth consistency between the PP and PS depth image is enforced through a regularization approach penalizing mistie between key reflectors in addition to the differential semblance misfit function. By migration / map demigration time information is obtained on the key reflectors of the PP and PS image. This time information, which is independent of the velocity model, can be map migrated to reconstruct the reflectors in depth for a given background model giving an automatic way to quantify the depth discrepancy in the tomographic approach. An approximative simplification uses the normal incidence point rays in the map migration. The method is presented in a general 3-D framework allowing for the use of true depth information such as well markers and the inclusion of anisotropy.

Methodology

The smooth background medium is described by the parameters given in the vector $\mathbf{m} = (m_1, \dots, m_n)$, which e.g. can be layer-based values or coefficients of a B-spline series expansion. The differential semblance misfit

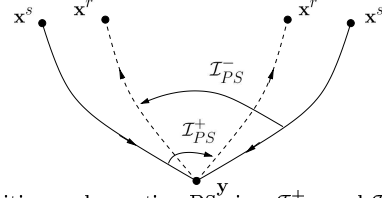


Fig. 1: Positive and negative PS cigs, \mathcal{I}_{PS}^+ and \mathcal{I}_{PS}^- . Arrows indicate the wavefield directions in the two reflection events. The solid and dashed curves are the P- and S-wave legs, respectively, of the different events. The source and receiver are denoted \mathbf{x}^s and \mathbf{x}^r , respectively.

function in angle measures the focusing ability of a cig. The optimum solution is found for uniform gathers. We denote the cigs from PP reflection events $\mathcal{I}_{PP}(\theta, \psi, \mathbf{y}; \mathbf{m})$ and the differential semblance measure for a given model on these cigs as $\mathcal{J}_{PP}(\mathbf{m})$. θ, ψ are the scattering and azimuth angles and $\mathbf{y} = (y_1, y_2, y_3)$ is the scattering point. Due to the diodic nature of PS reflections we split the contributing events to the cigs in the misfit function into a positive and negative part, denoted \mathcal{I}_{PS}^+ and \mathcal{I}_{PS}^- in analogy of positive and negative offsets in surface coordinates. The \mathcal{I}_{PS}^+ -cigs are computed with seismic events where the source and receiver rays intersect in the order of Figure 1 relative to the scattering angle and vice versa (opposite order of rays) for \mathcal{I}_{PS}^- . This splitting is necessary in a tomographic procedure as the rays, for the two cases, travel in different parts of the background model. Both \mathcal{I}_{PS}^+ and \mathcal{I}_{PS}^- are thus treated as separate cigs in the PS differential semblance misfit function denoted $\mathcal{J}_{PS}(\mathbf{m})$.

For the co-depting we interpret key reflectors which are geologically the same, but are imaged at different depths in the PP and PS images using an unacceptable model. Let the j 'th pair of interpreted key reflectors be given by

$$\{(y_1, y_2, z_{PP}^j(y_1, y_2; \mathbf{m})), (y_1, y_2, z_{PS}^j(y_1, y_2; \mathbf{m}))\}. \quad (1)$$

To enable an automatic matching of these key reflectors in depth, we demigrate the chosen reflectors to obtain time information which is independent of any background model and can be considered 'data'. As a simplification, we demigrate along normal incidence point (NIP) rays only. The two-way traveltime for the PP reflection events by demigration of the j 'th reflector from \mathbf{y} along the NIP ray to the surface point \mathbf{x} is denoted $\tau_{PP}^j(\mathbf{x})$. Using this time information we can map migrate to obtain the depth of the key reflector for every suggested background model

Depth consistent PP and PS tomography

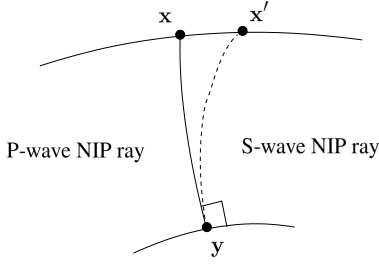


Fig. 2: Two NIP rays for the P and S wave from the subsurface point \mathbf{y} .

(Gjøystdal and Ursin, 1981)

$$(\mathbf{x}, \tau_{PP}^j(\mathbf{x})) \xrightarrow{\mathbf{m}} (y_1, y_2, z^j(y_1, y_2; \tau_{PP}^j(\mathbf{x}), \mathbf{m})). \quad (2)$$

To enable simple map migration of the reflectors of the PS image we construct pure mode SS traveltimes by resolving the P-leg of the PS events by using the PP traveltimes. In a correct velocity model, for the PS event, the NIP P ray connects \mathbf{y} to \mathbf{x} and the NIP S-ray connects \mathbf{y} to \mathbf{x}' , as in Figure 2. The dotted line indicate the S-wave ray while the solid line indicate the P-wave ray. The two-way PS traveltime τ_{PS} is then given by,

$$\tau_{PS}(\mathbf{x}, \mathbf{x}') = \tau_{PP}(\mathbf{x})/2 + \tau_{SS}(\mathbf{x}')/2, \quad (3)$$

with reflection point \mathbf{y} , where $\tau_{SS}(\mathbf{x}')$ is the SS two-way traveltime along the S-wave NIP ray. Notice in the use of two arguments in the two-way PS traveltime function as there are two points of emergence at the acquisition surface: Zero scattering angle does not imply zero offset.

In the unacceptable model, the PS event is imaged at \mathbf{y}' , while the PP event is imaged at \mathbf{y} , assuming the same \mathbf{x} position for the NIP P-ray through map demigration; the PS event tied to the PS image has two-way traveltime $\tau_{PS}(\mathbf{x}, \mathbf{x}'')$ ($\mathbf{x}' \neq \mathbf{x}''$ as the model is unacceptable). The zero scattering angle PP and PS two-way traveltimes are ‘data’ obtained from map demigration, and are considered to be correct. If we assume that $\mathbf{x}'' \approx \mathbf{x}'$, we can use (3) to compute $\tau_{SS}(\mathbf{x}'')$,

$$\tau_{SS}(\mathbf{x}'') \approx 2\tau_{PS}(\mathbf{x}, \mathbf{x}'') - \tau_{PP}(\mathbf{x}), \quad (4)$$

which is the NIP ray approximation of Gretchka and Tsvankin’s ‘PP+PS=SS’-procedure (2002). Using the pure mode $\tau_{PP}(\mathbf{x})$ and $\tau_{SS}(\mathbf{x}'')$ we map migrate the reflectors to depth enabling us to quantify the misfit in depth given the current background model as in equation (2). Notice that map migration of each set of these traveltime functions depends only on the background model parameters governing the particular mode. Notice also that the reflectors can be matched to other sources of depth information such as well logs. We denote the misfit function for depth mismatch of key reflectors $\mathcal{J}_D(\mathbf{m})$ and arrive at the joint angle tomography and co-depthing misfit functional,

$$\mathcal{J}(\mathbf{m}) = \lambda_1 \mathcal{J}_{PP}(\mathbf{m}) + \lambda_2 \mathcal{J}_{PS}(\mathbf{m}) + \mu \mathcal{J}_D(\mathbf{m}), \quad (5)$$

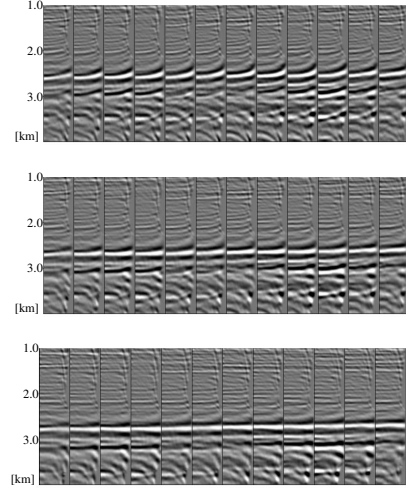


Fig. 3: The common-image point gathers of the isotropic P-wave velocity optimization after 0, 4 and 7 iterations.

where λ_1, λ_2 and μ are regularization parameters governing the trade-off between uniform cigs and depth consistency. By setting $\mu = 0$ the search aims at matching the range of the PP and PS forward scattering operators to the relevant data constituents by uniform cigs. The co-depthing is accomplished by setting $\mu \gg \lambda_1, \lambda_2 > 0$ and aims at a search in model space without changing the range of the forward scattering operators.

Strategy

We consider a transversely isotropic (TI) medium with a known direction of the symmetry axis, but disregard any azimuthal anisotropy. The medium is equivalent to a TI medium with a vertical symmetry axis (VTI) through the Bond transformation. Thus the medium is described by 4 parameters, for example the vertical P- and S-wave velocities v_{P0}, v_{S0} and Thomsen’s δ and ϵ . We approach the problem of estimating a velocity model in the framework of TI media considering a North Sea OBS dataset. This is performed with model updates in a step-wise manner, similar to (Sollid and Ettrich, 1999), using the following steps reflecting a hierarchy of model complexity; the misfit functional is given in (5):

- (i) We first carry out isotropic P-wave velocity analysis on PP cigs using differential semblance in angle ($\lambda_1 = 1, \lambda_2 = 0, \mu = 0$). Figure 3 shows 3 sets of PP cigs at iteration 0, 4 and 7 in the velocity update using a quasi-Newton approach (see (Brandsberg-Dahl et al., 2003) for details). The cigs are sampled every 250 meters from 1250 meters in the model with incoming scattering angle ranging from 0 to 45 degrees.
- (ii) Keeping the P-wave velocity model obtained in (i) fixed, we carry out isotropic S-wave velocity analysis

Depth consistent PP and PS tomography

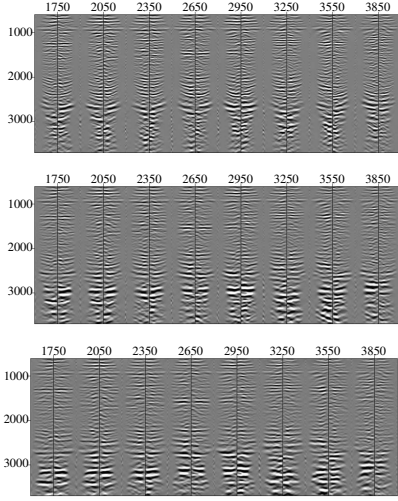


Fig. 4: The common-image point gathers of the isotropic S-wave velocity optimization after 0, 2 and 5 iterations.

on PS cigs using differential semblance in angle ($\lambda_1 = 0$, $\lambda_2 = 1$, $\mu = 0$). Figure 4 shows the flattening of the positive and negative PS cigs plotted back-to-back with angles ranging from 0.5 to 24 degrees outgoing S-wave angle (contrary to convention).

- (iii) We carry out seismic interpretation of the PP and PS images for key reflectors, and pick them. We use three reflectors of both images evenly distributed in depth denoted $\{(z_{PP}^1, z_{PS}^1), (z_{PP}^2, z_{PS}^2), (z_{PP}^3, z_{PS}^3)\}$ (suppressing the horizontal coordinates in equation (1)). We map demigrate these making use of the P- and S-wave velocity models obtained in (i) and (ii), and obtain PP and SS zero-offset traveltimes horizons, using equation (4), which play the role of ‘data’.
- (iv) We carry out co-depting by $\mathcal{J}_D(\mathbf{m})$, keeping the P-wave velocity model from (i) fixed using the PP reflector as ‘reference’, making use of map migration of the SS traveltimes data obtained in (iii). The contribution of the differential semblance misfit function plays the role of regularization ($\lambda_1 = 0$, $\mu \gg \lambda_2 > 0$). Figure 5 indicates the significant difference in the v_P/v_S -ratios resulting from (ii) and after co-depting, respectively, and is in large part attributed to the presence of anisotropy. Figure 6 shows a zoom of the deepest key reflector on three traces at 3.2 km in the model of the PP image (step (i)), the PS image step (ii) and the co-depted PS image, respectively. Observe that the key reflector z_{PS}^3 , with uniform gathers in the isotropic background model in step (ii), is moved several hundred meters to match the PP key reflector z_{PP}^3 .
- (v) After the isotropic processing steps (i) and (ii), the P- and S-wave velocities are approximately equal to

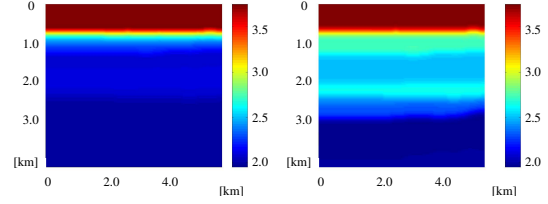


Fig. 5: v_p/v_s -ratios before and after co-depting, respectively.

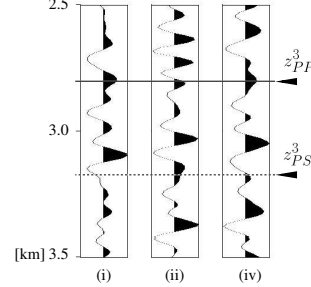


Fig. 6: Single traces, at 3200 m horizontal distance, from the isotropic PP images (step (i)), isotropic PS image before co-depting (step (ii)) and PS image after co-depting (step (iv)).

the NMO velocities;

$$\hat{v}_P \approx v_{PNMO} = v_{P0} \sqrt{1 + 2\delta} \quad (6)$$

and

$$\hat{v}_S \approx v_{SNMO} = v_{S0} \sqrt{1 + 2\sigma}, \quad \sigma = \left(\frac{v_{P0}}{v_{S0}} \right)^2 (\varepsilon - \delta). \quad (7)$$

The S-wave NMO velocity depends on the relationship $(\varepsilon - \delta)$ which is scaled by the squared v_{P0}/v_{S0} ratio through the σ parameter. It is well known that due to this, the processing of PS events is much more sensitive to the presence of anisotropy than that of PP events, but we are unable to resolve both parameters solely from PS data. Estimating the δ parameter requires well logs, large offset PP data or other information concerning depths of reflectors, as discussed by Audebert *et al.* (2001). If well log information is present the true depth of the reflectors can be obtained where the wells penetrate them. If no such information is present we simply choose $\delta = 0$. The true depth of a reflector – in the absence of too strong lateral heterogeneity – is governed by the v_{P0} parameter, the vertical P-wave velocity, which can be obtained by matching the PP reflectors to well markers by map migration. From step (i) our P-wave velocity \hat{v}_P , is close to the NMO velocity (6) while the S-wave velocity \hat{v}_S , after co-depting (iv) is close to the vertical S-wave velocity, but biased by the δ -parameter being matched to the PP image; that is

$$\hat{v}_S \approx v_{S0} \sqrt{1 + 2\delta}. \quad (8)$$

Depth consistent PP and PS tomography

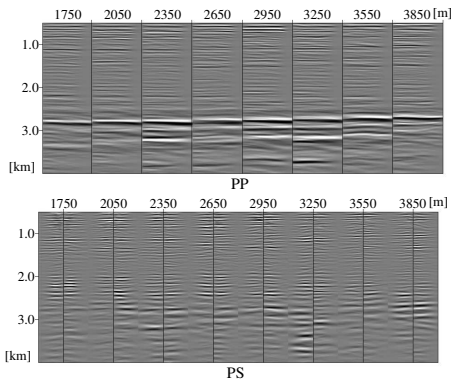


Fig. 7: Final PP and PS cigs after anisotropic model update obtained following a top-down approach.

When estimating ε and δ we keep \hat{v}_P and \hat{v}_S fixed and compute v_{P0} and v_{S0} from equation (6) and (8) for each value of δ . Using a top-down approach we carry out differential semblance in angle and semblance optimization of PP and PS cigs jointly admitting the model to become anisotropic (VTI); the co-depthing misfit plays the role of regularization ($\lambda_1, \lambda_2 \gg \mu > 0$). The resulting PP and PS cigs and images are given in Figure 7 and Figure 8. Indicated on the PP image are the three PP key reflectors used for co-depthing. These are also superimposed on the PS image for comparison.

Conclusion

The presented strategy enables depth consistent PP and PS imaging in a TI media. However, it is heavily dependent on our ability to interpret and pair geologically equivalent reflectors. This requires that good quality initial PS images can be computed. As the co-depthing procedure enables improved estimates of local the v_p/v_s -ratios, one potential use is within pore pressure prediction.

Acknowledgement

We thank Statoil for the use of the North Sea OBS data set, Børge Arntsen for data handling and Anders Sollid for discussions. S.-K. Foss thanks the URE-project, NTNU, for financial support.

References

Audebert, F., Granger, P.-Y., Gereau, C., and Herrenschmidt, A., 2001, Can joint PP and PS velocity analysis manage to corner δ , the anisotropic depthing parameter?: Proceedings 69th Ann. Internat. Mtg., Soc. Explor. Geophys., pages 145–148.

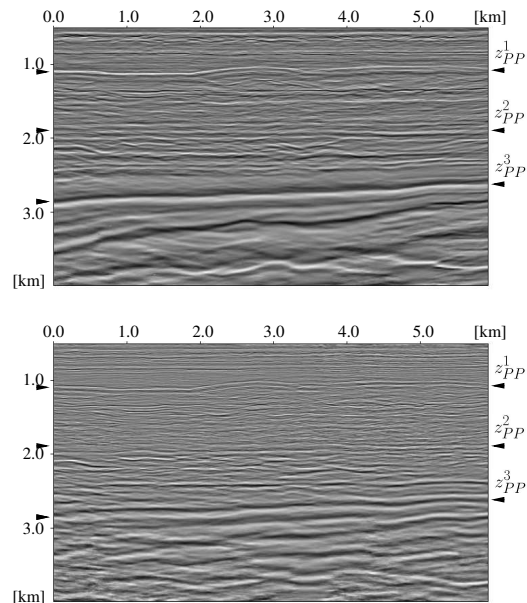


Fig. 8: Final PP image (top) and PS image (bottom), using the anisotropic parameters.

Brandsberg-Dahl, S., Ursin, B., and de Hoop, M. V., 2003, Seismic velocity analysis in the scattering angle/azimuth domain: Geophysical Prospecting, **51**, 295–314.

Gjøystdal, H., and Ursin, B., 1981, Inversion of reflection times in three-dimensions: Geophysics, **46**, 972–983.

Grechka, V., and Tsvankin, I., 2002, PP + PS = SS: Geophysics, **67**, 1961–1971.

Sollid, A., and Etrich, N., 1999, Coherency optimization of transversely isotropic velocity models via PP/PS prestack migration: Proceedings 69th Ann. Internat. Mtg., Soc. Explor. Geophys., pages 1707–1710.

Symes, W., and Carazzone, J., 1991, Velocity inversion by differential semblance optimization: Geophysics, **56**, 654–663.